1-2-2021

Novel approach of electroshock treatment for defect repair in near-β titanium alloy manufactured via directed energy deposition

Lechun Xie

Haojie Guo

Yanli Song

Lin Hua

Liqiang Wang

See next page for additional authors

10.1007/s11661-020-06098-0

Xie, L., Guo, H., Song, Y., Hua, L., Wang, L., & Zhang, L. C. (2021). Novel approach of electroshock treatment for defect repair in near-β titanium alloy manufactured via directed energy deposition. *Metallurgical and Materials Transactions A, 52*(2), 457-461. https://doi.org/10.1007/s11661-020-06098-0

Communication

Novel Approach of Electroshock Treatment for Defect Repair in Near-β Titanium Alloy Manufactured *via* Directed Energy Deposition

LECHUN XIE, HAOJIE GUO, YANLI SONG, LIN HUA, LIQIANG WANG, and LAI-CHANG ZHANG

A subsecond and novel approach of electroshock treatment (EST) is used in this study to repair defects in directed-energy-deposited Ti-5Al-5Mo-5V-3Cr-1Zr near-β titanium alloy. After EST, the porosity of the specimen decreased significantly from 0.81 to 0.1 pct. Large cracks observed at the bottom of the above mentioned near-β titanium alloy became intermittent small cracks and the number of voids decreased. The defects in the top and middle regions of the specimens are repaired. The potential defect repair is attributable to energy concentration, which promoted the coalescence of defect tips, and thermal stresses, which compressed the defects inward and closed them.

https://doi.org/10.1007/s11661-020-06098-0

As an additive manufacturing (AM) technology, directed energy deposition (DED) is based on a digital model and adopts a layer-by-layer deposition to manufacture a component.[1–6] DED can significantly shorten the product development cycle, reduce costs, and improve manufacturing efficiency by controlling the parameters. The manufacture of near-β titanium alloy is sensitive to the casting parameters, rendering the forging and machining of complex components difficult.[7] Therefore, DED provides a useful approach for manufacturing complex near-β titanium components. However, owing to the short interaction time between laser and metal powders and the fast heating and cooling of materials during laser-based DED, internal defects, such as voids, cracks, or unmelted powders, are typically observed in as-built components, thereby affecting the performance of directed-energy-deposited components.[8–10] The effects of these manufacturing defects differ from the favorable performances of designed porous scaffolds.[11,12] As reported previously, large defects (> 1 mm) in directed-energy-deposited 304L stainless steel significantly reduced both the ultimate tensile strength and ductility as well as accelerated fatigue crack initiation.[9] In the AM of Ti-6Al-4V, the defect size and distribution affected its mechanical properties,[8] whereas the existence of pores reduced the elongation and the fatigue strength by 60 and 33 pct, respectively, compared with a specimen with no pores.[13]

To reduce and eliminate defects, two popular approaches were adopted: (1) optimizing the parameters used in DED and (2) performing post-treatments to repair defects. Studies have been performed based on approach (1), in which the laser power and feeding rate were optimized[14] to investigate the dynamic competition between bubble explosion and solidification[15] and analyze defect data collected from an inspection device;[16] furthermore, a control scheme based on temperature feedback data was used.[17] In the AM of near-β titanium alloy, relatively high-density Ti-5Al-5Mo-5V-3Cr (Ti-5553) was achieved by manipulating the laser power and scanning strategy using laser powder bed fusion technology,[18–20] and a Ti-5553 specimen with a relative density of 99.92 pct was manufactured.[19] It was discovered that the laser power, feeding rate, and scanning speed were the main parameters affecting the integrity and quality of the deposited Ti-5553 alloy.[20] Based on the previous discussion, it is clear that approach (1) is beneficial for manufacturing a material with a particular shape and structure. However, for different materials with complex shapes and structures, the adjustment of deposition parameters is inevitable, which would result in a lower efficiency during practical engineering manufacturing. Moreover, it is difficult to control the defects and stress in large and complex components. Consequently, post-treatments using approach (2) may offer advantages in repairing defects and eliminating residual stresses during practical engineering manufacturing.

Heat treatment was used to optimize the performance of laser-based directed-energy-deposited titanium alloys. The microstructure of directed-energy-deposited Ti-

LECHUN XIE, HAOJIE GUO, YANLI SONG, and LIN HUA are with the Hubei Key Laboratory of Advanced Technology for Automotive Components, Wuhan University of Technology, Wuhan 430070, P.R. China and also with the Hubei Collaborative Innovation Center for Automotive Components Technology, Wuhan University of Technology, Wuhan 430070, P.R. China. Contact e-mails: xielechun@whut.edu.cn; hualin@whut.edu.cn LIQIANG WANG is with the State Key Laboratory of Metal Matrix Composites, School of Materials Science and Engineering, Shanghai Jiao Tong University, No. 800 Dongchuan Road, Shanghai 200240, P.R. China. Contact e-mail: wang_liqiang@sjtu.edu.cn LAI-CHANG ZHANG is with the School of Engineering, Edith Cowan University, Joondalup, 270 Joondalup Drive, Perth, WA 6027, Australia.

Lechun Xie and Haojie Guo contributed equally.

Manuscript submitted May 5, 2020; accepted November 2, 2020.

Article published online January 2, 2021

5553 was manipulated *via in-situ* laser annealing.[21] After heat treatment, the porosity of the selective laser-melted Ti-5553 decreased.[22,23] Herringbone grain boundaries were formed in laser-based directed-energy-deposited Ti-5Al-5Mo-5V-1Cr-1Fe (Ti-55511), which effectively inhibited crack propagation.[24] Moreover, it was reported that the defects and residual stresses in other directed-energy-deposited alloys decreased owing to heat treatment and hot isostatic pressing.[25–28] Although heat treatment can reduce and eliminate internal defects in directed-energy-deposited components, the treatment process is specified for the entire component and targeted defects in the interior of the specimens are difficult to repair. The lengthy processing time and the complicated equipment required for heat treatment restrict its application in certain practical conditions; therefore, a more convenient processing technology that can effectively and rapidly repair defects in directed-energy-deposited components should be developed.

Electroshock treatment (EST)[29,30] is a new type of postprocessing technology developed based on the traditional electric pulse treatment. Researchers have adopted the traditional electric pulse treatment to repair cracks owing to its instantaneous heating and nonequilibrium treatment.[31,32] The mechanism was ascribed to the thermal and nonthermal effects of electrical pulse processing[33,34] and the atom migration promoted by the increased driving force of the phase transition around microcracks.[35] Compared with the traditional electric pulse treatment, EST offers a higher electrodensity and a more stable pulse current. Moreover, EST is suitable for the treatment of bulk materials and large components. Consequently, EST can be applied to repair defects in a laser-based directed-energy-deposited near-β titanium alloy and is expected to provide insights into defect repair in additive-manufactured titanium alloys.

In this study, laser-deposited Ti-5Al-5Mo-5V-3Cr-1Zr (Ti-55531) alloy was treated *via* EST; subsequently, its microstructural variations were characterized *via* scanning electron microscopy (SEM), and the position and tomography of its defects were detected *via* X-ray computed tomography (X-CT).

The laser-based DED of Ti-55531 alloy was performed using the Optomec LENS MR-7 system. Ti-55531 powder with a diameter of 45 to 150 μm was obtained *via* plasma rotating electrode process atomization. The DED was performed under argon protection with an oxygen content of < 20 ppm. The deposition parameters were as follows: laser power of 225 W, scanning speed of 25 mm/s, and incremental step of *Z*-axis of 0.254 mm. The specimens were deposited on a Ti-55531 substrate with 20-mm thickness, and the scan pattern shown in Figure 1(a) was adopted. Cylindrical specimens with a diameter of 5 mm and a height of 10 mm were deposited, as shown in Figure 1(b). To conduct the EST experiment, burrs and excess powder on the surface of the specimen were removed and the top and bottom surfaces of the specimen were ground and polished to provide good contact with the electrodes. During the EST, the specimen was placed between the upper and lower electrodes in the EST equipment. The pulse voltage was 7.8×10^3 V, monitored using a Hall current sensor (in Figure 1(b)); the current amplitude and density were 4.5×10^3 A and 2.3×10^4 A/cm^2, respectively, and the EST was performed for 0.04 seconds. The detailed process of the EST is available in References 29 and 30.

Currently, X-CT is the most widely used nondestructive testing technology.[36,37] A schematic of the X-CT system is shown in Figure 1(c); an X-ray is passed through the rotating specimen, whereas the intensity variation is measured and recorded by the detector. According to the intensity variation and computer reconstruction, the distribution of internal defects in specimens, such as voids, pores, and cracks, can be shown clearly and accurately. A high-resolution X-CT

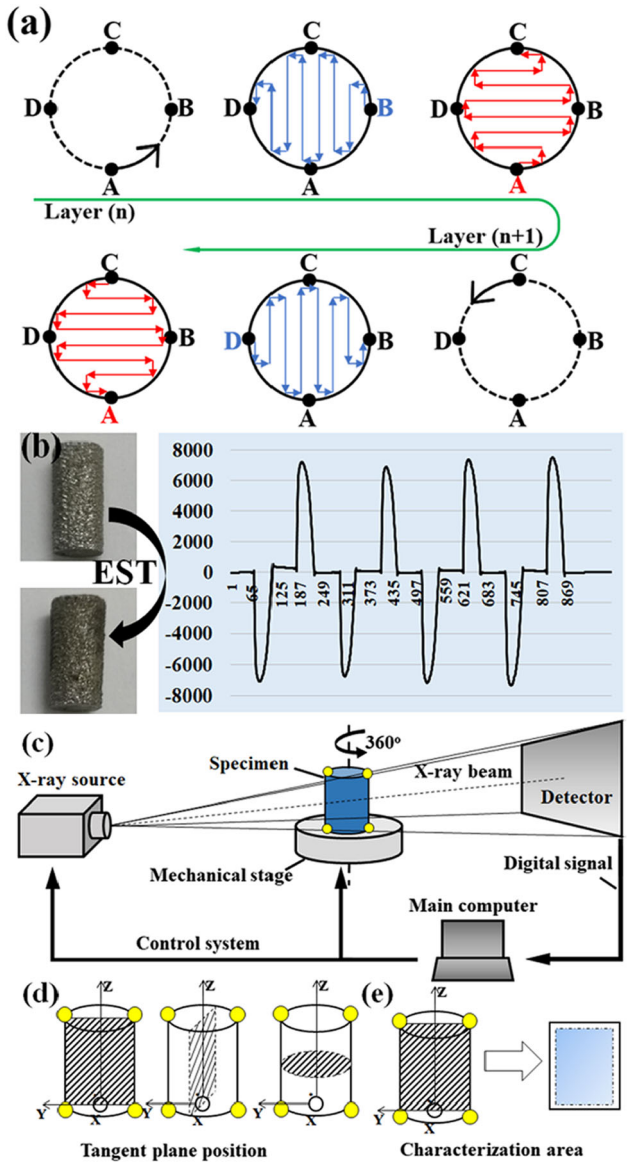

Fig. 1—(*a*) Scan pattern of the cylindrical specimen; (*b*) specimens before and after EST and pulse voltage monitored using the Hall current sensor; (*c*) schematic diagram of the X-CT system; (*d*) *YZ*, *XZ*, and *XY* tangent planes; and (*e*) characterization area of the microstructure.

system (CD-300BX, Chongqing, China) was used to detect the defects in the directed-energy-deposited Ti-55531 specimen before and after the EST. The scans were performed at 80 kV and 400 μA at a 10-μm resolution, the exposure time for each image was 500 ms, and the spatial resolution was five line pairs per millimeter. A three-dimensional (3-D) computer reconstruction was performed using VGStudio software for analysis. To ensure the detection of defects before and after the EST, one central plane (*YZ*) determined using four special points on the specimen was indicated (as shown in Figure 1(d)), whereas the positions of selected tangent planes *YZ*, *XZ*, and *XY* were determined. The microstructure was characterized *via* SEM (Zeiss Ultra Plus, Germany) on the *YZ* plane, as shown in Figure 1(e). Before microstructure characterization, standard metallographic grinding and polishing methods were used; subsequently, the specimens were etched in a solution with a volume ratio of $HF:HNO_3:H_2O$ = 3:5:92 at room temperature.

The variation of defects evaluated *via* X-CT before and after the EST are shown in Figure 2. The two-dimensional (2-D) size and distribution of defects in three tangent planes (*YZ*, *XZ*, and *XY*), which were obtained from the 3-D reconstruction, are shown in Figure 2(a); the dark region represents the defects. Defects with irregular shapes, such as voids and cracks (marked by arrows in Figure 2(a)), were observed at the bottom of the specimen. Some small defects were observed in the middle, and a few defects were observed at the top. During the laser-based DED, the powders melted and solidified rapidly and there was not enough time for gas in the molten pool to be released, so it was entrapped, causing defects during the fast cooling of the deposited specimen.[14,15,38] The cooling rate was high at the top surface; however, the cooling rates between the bottom and top regions differed. In a previous study,[38] *in situ* thermal monitoring of a titanium alloy during DED was performed and the cooling rates were calculated based on experimental data, verifying that the initial cooling rate in the bottom region was higher than that at the top region. The different cooling rates might have contributed to the formation of defects. In addition, tensile residual stresses were introduced by the fast cooling of the specimen, which resulted in the formation of cracks at the bottom of the specimen.[14,39] This is attributable to the faster cooling rate in the bottom region due to the connection between the specimen and the substrate.[38]

After the EST, X-CT was performed using the *XYZ* coordinate system and the same processing parameters used before the EST. The X-CT results of the treated specimen are shown in Figure 2(b); as shown, some large defects, such as voids, decreased in size and some small defects, such as cracks, were repaired in the bottom region. The *XY* plane is located in the middle of the cylindrical sample, as shown in Figures 1(d) and (e). In the middle and top regions, the original defects were almost completely repaired after the EST. To evaluate the defects quantitatively, the porosity determined from statistical analysis is shown in Figure 2(c). To determine the porosity, the position and contour of defects were first detected *via* X-CT. Subsequently, 3-D computer reconstruction was performed using VGStudio software, and the volume of each void and crack was calculated. Finally, the volume of all defects was summed and the porosity was obtained. The original porosity of the directed-energy-deposited Ti-55531 specimen (0.81 pct) decreased significantly to 0.1 pct after the EST, implying that the defects of voids and cracks were repaired effectively *via* the EST. The microstructure characterization shown in Figure 3 verifies the results.

The microstructure of the *YZ* plane (in Figure 2) was characterized *via* SEM, and the size and distribution of the defects from the top (T) to bottom (B) regions are shown in Figure 3. It is noteworthy that during the X-CT experiments, the same specimen was used before and after the EST; therefore, the images shown in Figure 2 were obtained from the same specimen. After the EST was performed, the microstructure was characterized, as shown in Figure 3(b). However, the cross-sectional images of the specimen before the EST (shown in Figure 3(a)) were obtained from another specimen that was manufactured using the same DED parameters. Prior to the EST, some small cracks and irregular small voids were observed in the T and middle (M) regions (as

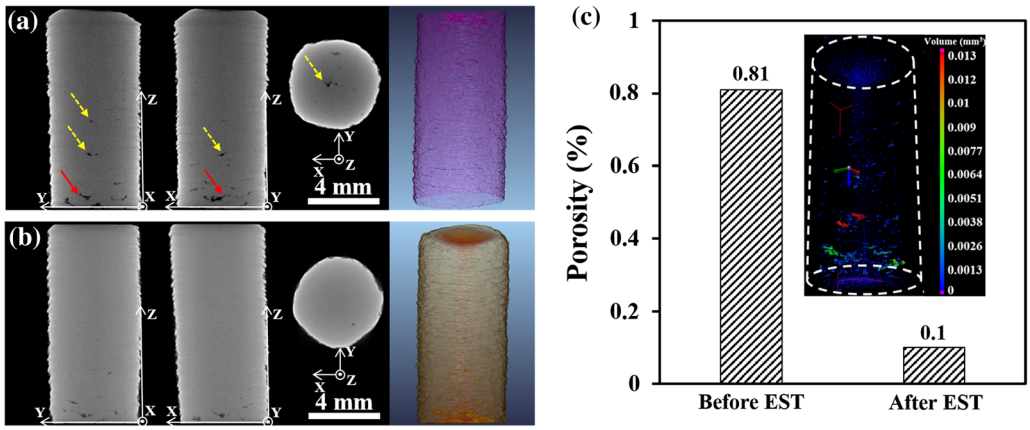

Fig. 2—X-CT results of 2-D size and distribution of defects in three tangent planes (*YZ*, *XZ*, and *XY*) and the 3-D reconstruction (*a*) before and (*b*) after EST; (*c*) porosity of the specimen before and after EST.

shown in Figure 3(a)). However, in the B region, a large number of cracks and voids were formed, consistent with the X-CT results shown in Figure 2(a). Because of the significant temperature difference between the substrate and the molten pool, defects and residual stresses tended to form within the first few layers.[38] The formation of pores, which is related to bubble retention and rejection from solution, is complicated.[15] The molten pool has a free surface where gas can escape. However, in the interface between the molten pool and the solidification part, some powders may not be melted thoroughly because of the fast cooling rate; hence, bubbles may be introduced during solidification and then remain to form pores. Moreover, during the later stage of solidification, residual stresses may result in local deformation and cracks may form along the interface between the two deposition layers, particularly in the bottom region of the specimen. After the EST, no defects were observed in the T region and fewer cracks appeared in the M position, as shown in Figure 3(b). Moreover, an apparent repair of defects was observed in the B region, and no continuous long cracks were observed. The tips of the long cracks were closed, and long cracks became intermittent small cracks. The size and number of voids reduced significantly, and the ends of the voids transformed from sharp angles to elliptical arcs, which illustrate the repairing effect of EST on defects. The potential mechanisms of repairing defects *via* EST are discussed subsequently and shown in Figure 4.

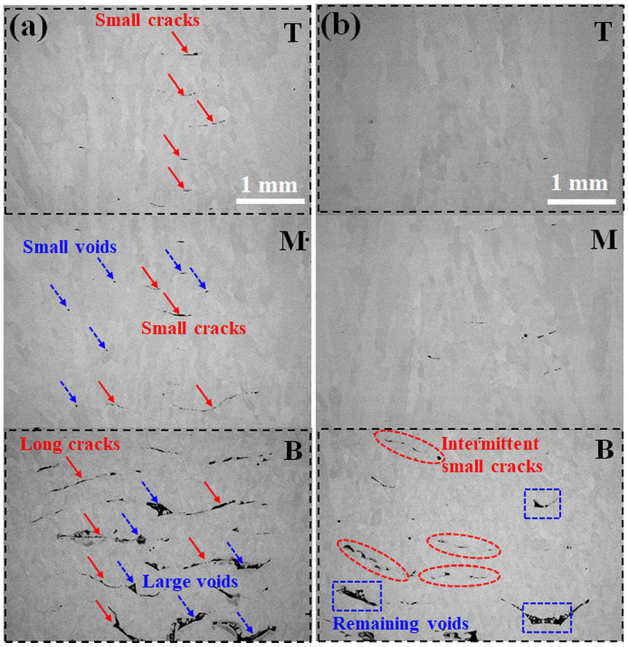

Fig. 3—Microstructure of defects corresponding to the tangent plane of *YZ* from T to B regions: (*a*) before EST and (*b*) after EST.

The preceding results indicate that EST can repair the defects in directed-energy-deposited Ti-55531 in subseconds, and the potential mechanisms are ascribed to the thermal effect and current crowding effect, as shown in Figure 4. The thermal effect is based on Joule heating,[40] which is caused by electrical resistance and results in an increase in the temperature of the entire specimen; this is a typical phenomenon in metals (Figure 4(a)). Uniform heating occurs only when uniform continuity exists in a material (no defects). For a material with defects, the current is not uniform as it passes around the defects due to the current crowding effect resulting from the different current flow and resistances between defects and the material.[41–43] The pulse current under an EST tends to pass through the region with a smaller resistance, and more energy is concentrated on the tips of the defects (Figure 4(b)). The current crowding effect is an interaction between electric fields and thermal effects, resulting in localized heating at the defects. Under the thermal effect, Joule heat is generated on the tips of voids and cracks, whereas under the current crowding effect, the current density increases the energy concentration on the tips of voids and cracks (Figure 4(c)). In this case, the material around the tips of defects is hotter, resulting in a local hydrostatic compression due to thermal expansion. Consequently, it is prone to softening and deformation, thereby promoting the closing of the defect tips[44] and the repair of voids and cracks (Figure 4(d)). By combining the thermal and current crowding effects, most of the cracks and voids are repaired completely, whereas some large cracks become intermittent small cracks and some voids

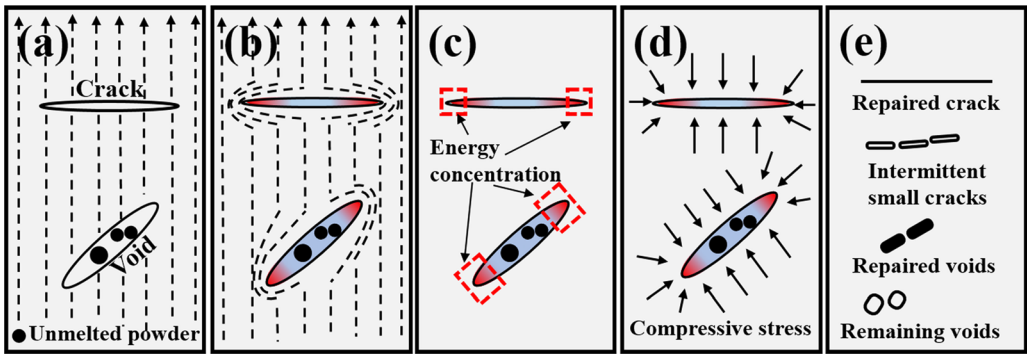

Fig. 4—Potential mechanism of defect repair *via* EST: (*a*) thermal effect, (*b*) current crowding effect, (*c*) energy concentration, (*d*) compressive effect by thermal stress, and (*e*) completely and partially repaired defects.

are only partially reduced because of the limited energy of EST (Figure 4(e)). The preceding results and discussion indicate that the defects of directed-energy-deposited Ti-55531 were repaired *via* EST in a much shorter time compared with traditional heat treatment. EST can realize efficient energy usage and shorten the processing time; hence, it is apromising method for repairing defects in directed-energy-deposited near-β titanium alloys.

In summary, the defects in laser-based directed-energy-deposited Ti-55531 alloy were repaired effectively *via* EST in less than 1 second, and the porosity of the sample reduced from 0.81 to 0.1 pct after the EST. After the EST, no defects were observed in the T region and fewer cracks appeared in the M region. The continuous long cracks observed truncated to intermittent small cracks in the B region. The defect repair was attributable to the energy concentration at the defects, which promoted the coalescence of the defect tips, and the compressive effect of thermal stresses, which compressed the material surrounding the defects, hence closing and repairing them. This study demonstrated that EST can repair many types of defects in directed-energy-deposited near-β titanium alloy; hence, it is a feasible method for modifying the structure of additive-manufactured titanium alloys.

This study was financially supported by the National Natural Science Foundation of China (Grant Nos. 51901165 and 51975441), the Fundamental Research Funds for the Central Universities (Grant Nos. WUT 2018IVA063, WUT 2018IVA064, and 205207013), the "Chu Tian Scholar" project of Hubei Province (Grant No. CTXZ2017-05), the 111 Project (Grant No. B17034), and the Innovative Research Team Development Program of Ministry of Education of China (Grant No. IRT_17R83). We thank Dr. Yanping Lu for the assistance with X-CT characterization.

REFERENCES

1. Z. Zhao, J. Chen, H. Tan, G. Zhang, X. Lin, and W. Huang: *Scripta Mater*., 2018, vol. 146, pp. 187–91.
2. J.H. Martin, B.D. Yahata, J.M. Hundley, J.A. Mayer, T.A. Schaedler, and T.M. Pollock: *Nature*, 2017, vol. 549, p. 365.
3. H. Hou, E. Simsek, T. Ma, N.S. Johnson, S. Qian, C. Cisse, D. Stasak, N.A. Hasan, L. Zhou, and Y. Hwang: *Science*, 2019, vol. 366, pp. 1116–21.
4. Y.-J. Liang, D. Liu, and H.-M. Wang: *Scripta Mater*., 2014, vol. 74, pp. 80–83.
5. N. Shamsaei, A. Yadollahi, L. Bian, and S.M. Thompson: *Addit. Manuf*., 2015, vol. 8, pp. 12–35.
6. S.M. Thompson, L. Bian, N. Shamsaei, and A. Yadollahi: *Addit. Manuf*., 2015, vol. 8, pp. 36–62.
7. N. Jones, R. Dashwood, D. Dye, and M. Jackson: *Metall. Mater. Trans. A*, 2009, vol. 40A, pp. 1944–54.
8. J.W. Pegues, S. Shao, N. Shamsaei, N. Sanaei, A. Fatemi, D.H. Warner, P. Li, and N. Phan: *Int. J. Fatigue*, 2020, vol. 132, p. 105358.
9. T.R. Smith, J.D. Sugar, J.M. Schoenung, and C. San Marchi: *Mater. Sci. Eng. A*, 2019, vol. 765, p. 138268.
10. L. Li: *J. Mater. Sci*., 2006, vol. 41, pp. 7886–93.
11. S. Liu, J. Liu, L. Wang, R.L. Ma, Y. Zhong, W. Lu, and L. Zhang: *Scripta Mater*., 2020, vol. 181, pp. 121–26.
12. L.-C. Zhang, L.-Y. Chen, and L. Wang: *Adv. Eng. Mater*., 2020, vol. 22, p. 1901258.
13. R. Biswal, X. Zhang, A.K. Syed, M. Awd, J. Ding, F. Walther, and S. Williams: *Int. J. Fatigue*, 2019, vol. 122, pp. 208–17.
14. D. Masaylo, S. Igoshin, A. Popovich, and V. Popovich: *Mater. Today Proc*., 2020.
15. P. Zhang, X. Zhou, X. Cheng, H. Sun, H. Ma, and Y. Li: *Addit. Manuf*., 2020, vol. 32, p. 101026.
16. R. Reese, H. Bheda, and W. Mondesir: U.S. Patent No. 10,421,267, 2019.
17. S. Das, R. Bansal, and J. Gambone: U.S. Patent No. 9,522,426, 2016.
18. C. Zopp, S. Blümer, F. Schubert, and L. Kroll: *Ain Shams Eng. J*., 2017, vol. 8, pp. 475–79.
19. S. Bakhshivash, H. Asgari, P. Russo, C. Dibia, M. Ansari, A. Gerlich, and E. Toyserkani: *Int. J. Adv. Manuf. Technol*., 2019, pp. 1–11.
20. A. Hatefi: *School of Metallurgy and Materials*, University of Birmingham, Birmingham, 2013.
21. C. Qiu, G.A. Ravi, and M.M. Attallah: *Mater. Des*., 2015, vol. 81, pp. 21–30.
22. H.D. Carlton, K.D. Klein, and J.W. Elmer: *Sci. Technol. Weld. Join*., 2019, pp. 1–9.
23. H. Schwab, M. Bönisch, L. Giebeler, T. Gustmann, J. Eckert, and U. Kühn: *Mater. Des*., 2017, vol. 130, pp. 83–89.
24. C. Liu, L. Yu, A. Zhang, X. Tian, D. Liu, and S. Ma: *Mater. Sci. Eng. A*, 2016, vol. 673, pp. 185–92.
25. W. Tillmann, C. Schaak, J. Nellesen, M. Schaper, M. Aydinöz, and K.-P. Hoyer: *Addit. Manuf*., 2017, vol. 13, pp. 93–102.
26. X. Yuan, Q. Wei, S. Wen, and Y. Shi: *Hot Work. Technol*., 2014, vol. 4, p. 91.
27. P. Han, A. Tofangchi, A. Deshpande, S. Zhang, and K. Hsu: *Proc. Manuf*., 2019, vol. 34, pp. 672–77.
28. N.O. Larrosa, W. Wang, N. Read, M.H. Loretto, C. Evans, J. Carr, U. Tradowsky, M.M. Attallah, and P.J. Withers: *Theor. Appl. Fract. Mech*., 2018, vol. 98, pp. 123–33.
29. L. Xie, H. Guo, Y. Song, C. Liu, Z. Wang, L. Hua, L. Wang, and L.-C. Zhang: *Mater. Charact*., 2020, vol. 161, p. 110137.
30. L. Xie, C. Liu, Y. Song, H. Guo, Z. Wang, L. Hua, L. Wang, and L.-C. Zhang: *J. Mater. Res. Technol*., 2020, vol. 9, pp. 2455–66.
31. H. Song, Z. Wang, X. He, and J. Duan: *Sci. Rep*., 2017, vol. 7, p. 7097.
32. T. Yu, D. Deng, G. Wang, and H. Zhang: *J. Clean. Prod*., 2016, vol. 113, pp. 989–94.
33. Z. Lu, C. Guo, P. Li, Z. Wang, Y. Chang, G. Tang, and F. Jiang: *J. Alloys Compd*., 2017, vol. 708, pp. 834–43.
34. A. Hosoi, T. Nagahama, and Y. Ju: *Mater. Sci. Eng. A*, 2012, vol. 533, pp. 38–42.
35. Z. Lu, F. Jiang, Y. Cheng, C. Guo, H. Hou, and Y. Liu: *Suxing Gongcheng Xuebao*, 2015, vol. 22, pp. 117–27.
36. A. Karme, A. Kallonen, V.-P. Matilainen, H. Piili, and A. Salminen: *Phys. Procedia*, 2015, vol. 78, pp. 347–56.
37. H. Gong, V.K. Nadimpalli, K. Rafi, T. Starr, and B. Stucker: *Technologies*, 2019, vol. 7, p. 44.
38. G.J. Marshall, W.J. Young, S.M. Thompson, N. Shamsaei, S.R. Daniewicz, and S. Shao: *JOM*, 2016, vol. 68, pp. 778–90.
39. B.A. Szost, S. Terzi, F. Martina, D. Boisselier, A. Prytuliak, T. Pirling, M. Hofmann, and D.J. Jarvis: *Mater. Des*., 2016, vol. 89, pp. 559–67.
40. H. Conrad, N. Karam, and S. Mannan: *Scripta Metall*., 1984, vol. 18, pp. 275–80.
41. H. Conrad: *Mater. Sci. Eng. A*, 2000, vol. 287, pp. 276–87.
42. H. Conrad: *Mater. Sci. Eng. A*, 2000, vol. 287, pp. 227–37.
43. H. Conrad, N. Karam, and S. Mannan: *Scripta Metall*., 1983, vol. 17, pp. 411–16.
44. X. Du, B. Wang, and J. Guo: *J. Mater. Res*., 2007, vol. 22, pp. 1947–53.